

# Self-collimating photonic crystal polarization beam splitter

V. Zabelin, L. A. Dunbar, N. Le Thomas, and R. Houdré

*Institut de Photonique et d'Electronique Quantique, Ecole Polytechnique Fédérale de Lausanne (EPFL),  
Station 3, CH-1015 Lausanne, Switzerland*

M. V. Kotlyar, L. O'Faolain, and T. F. Krauss

*SUPA, School of Physics and Astronomy, University of St. Andrews, St. Andrews, Fife, KY16 9SS, UK*

Received October 20, 2006; accepted November 18, 2006;  
posted December 5, 2006 (Doc. ID 76079); published February 2, 2007

We present theoretical and experimental results of a polarization splitter device that consists of a photonic crystal (PhC) slab, which exhibits a large reflection coefficient for TE and a high transmission coefficient for TM polarization. The slab is embedded in a PhC tile operating in the self-collimation mode. Embedding the polarization-discriminating slab in a PhC with identical lattice symmetry suppresses the in-plane diffraction losses at the PhC–non-PhC interface. The optimization of the PhC–non-PhC interface is thereby decoupled from the optimization of the polarizing function. Transmissions as high as 35% for TM- and 30% for TE-polarized light are reported. © 2007 Optical Society of America  
OCIS codes: 130.3130, 230.3990, 230.3120, 230.5440, 230.1360.

Photonic crystals (PhCs) have been the focus of extensive research since their inception in the 1980s. Through skillful engineering, PhC heterostructures offer a variety of appealing optical functionalities, which may be integrated into an advanced photonic circuit chip as a building block with a very reduced footprint. Because of their small size, large refractive index contrast, and the very nature of the lattice, PhC structures are highly sensitive to the polarization of light, which offers opportunities for polarization control devices. Polarization splitters belong to such a class of devices, which can be of interest in a polarization diversity scheme where the two orthogonal polarization states of the signal are treated independently.

A polarization splitter is a more demanding device than a polarizer, as it should perform equally well for both polarizations. The key parameters to assess are transmission coefficients for both polarization outputs, which should be as close to unity as possible, and cross talk and backreflection, which should be as low as possible. Recently several types of polarization splitter, based on two-dimensional (2D) PhCs, have been proposed.<sup>1–8</sup> For example, the use of two coupled parallel waveguides with different coupling lengths for TE and TM polarized light allows the transfer of light with only the desired polarization from one waveguide to another.<sup>1,2</sup> One approach is based on polarization-dependent dispersion properties of PhCs, which lead to different propagation directions for TE and TM polarized light.<sup>3</sup> Exploiting this in a structure with positive refraction for one polarization and negative refraction for another allows the polarization to be split.<sup>4–6</sup> Another approach is based on the fact that the bandgaps for TE and TM polarizations occur at different wavelength ranges. It follows that an appropriate choice of parameters makes it possible for a given wavelength range to transmit the

TM polarization and to reflect the TE polarization. Straightforward implementation of such a concept, where a PhC slab, exhibiting a gap for only one polarization, is inserted into a regular or a PhC waveguide, proved to be inefficient. This is mainly because of the occurrence of strong in-plane light diffraction at the PhC interface for air-hole-based structures and out-of-plane scattering for pillar-based PhC structures. This makes such a device an acceptable polarizer but not a polarization splitter.

It is therefore desirable to distinguish between the two functions of injecting light into the lattice and splitting the two polarizations. To address the first function, it is well known that for specific frequencies and PhC lattice structures light can propagate without diffraction.<sup>9–11</sup> This effect, commonly referred to as self-collimation, relies on the special dispersion properties of Bloch waves in PhCs, where the curvature of the equifrequency surface departs from the normally circular curvature in free space. As the direction of a propagating Bloch mode is always normal to the equifrequency surface, self-collimation is achieved when the equifrequency surfaces are as flat as possible. For a low-index-contrast planar waveguide structure self-collimation has the desirable property that it occurs at nearly identical frequencies for both TE and TM polarizations and over a wide frequency range (several percent) for relatively short structures (several tens times the lattice constant). The second function of polarization splitting is realized by inserting a slab of the same lattice constant into the self-collimating structure, but with a different filling factor, which exhibits a large reflection coefficient for TE and a high transmission coefficient for TM polarized light. Note that the short path length of the TM light through the slab means that maintaining self-collimation in this region is not essential. Embedding the polarizing slab within a PhC

structure of the same crystal lattice (only the filling factor changes) suppresses the in-plane diffraction losses at the PhC/non-PhC interface. The optimization of the PhC interface is then decoupled from the optimization of the polarizer functionality. Figure 1 shows the gap map of a square lattice with an effective index  $n_{\text{eff}}=3.25$ . The shaded areas indicate the bandgap energies as a function of the filling factor ( $f$ ). The gray (black) curve shows the self-collimating frequency for TE (TM) polarization as a function of  $f$ . The operating points should be chosen such that for a given frequency the first lattice has a bandgap for one polarization but not for the other, whereas the second lattice exhibits self-collimation for both polarizations. Such a pair of operating points is indicated in Fig. 1 (points A and B). The frequency range of operation depends on the frequency width of the bandgap and is also related to the slope of the self-collimating curves; a steeper curve favors a wider operating range. A 5% frequency range, suitable for coarse WDM operation, is indicated in Fig. 1 (shaded segment). Figures 2(a1) and 2(a2), respectively, show 2D finite-difference time domain (FDTD) images of the TE and TM field patterns for the optimized self-collimating polarization splitter structure. Note the weak backreflection and the absence of in-plane diffraction. The optimized filling factor for a square lattice of holes was found to be  $f_{\text{sc}}=30\%$  for the self-collimating tile and  $f_{\text{pol}}=50\%$  for the polarizer slab (Fig. 3). Transmission for both polarizations of up to 83% is predicted, limited mainly by interface reflection, and occurs over a bandwidth as large as  $\Delta u/u = 7\%$  (shaded area in Fig. 3). As expected, the TM channel exhibits good transmission when the incident beam frequency lies within the photonic bandgap, and the TE channel exhibits transmission over a broader range that is limited either by the band edge of the TM bandgap or when the frequency deviates too much from the self-collimation conditions.

The fabricated structure consists of six lines with a nominal filling factor of  $f=50\%$  embedded in a tile of 40 unit cells with  $f=30\%$ . Refraction in the slab and Goos-Hänchen effects introduce a small offset of the output axis waveguides compared with their nominal

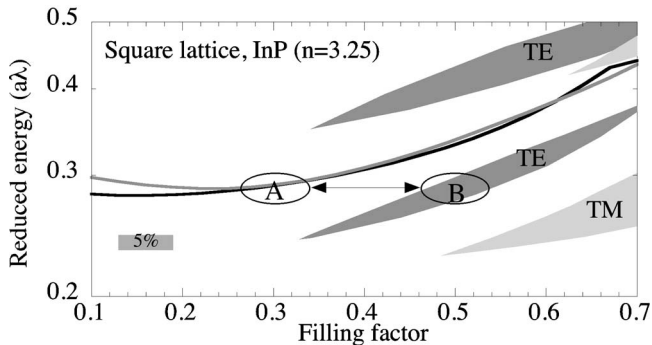


Fig. 1. Gap map of a square lattice of air holes in dielectric with an effective index  $n_{\text{eff}}=3.25$ . The shaded areas indicate the bandgap energies. The black (gray) curve shows the self-collimating frequency for TM (TE) polarization. A pair of operating points are indicated (A and B). The shaded segment indicates a 5% operating range, corresponding to coarse WDM operation.

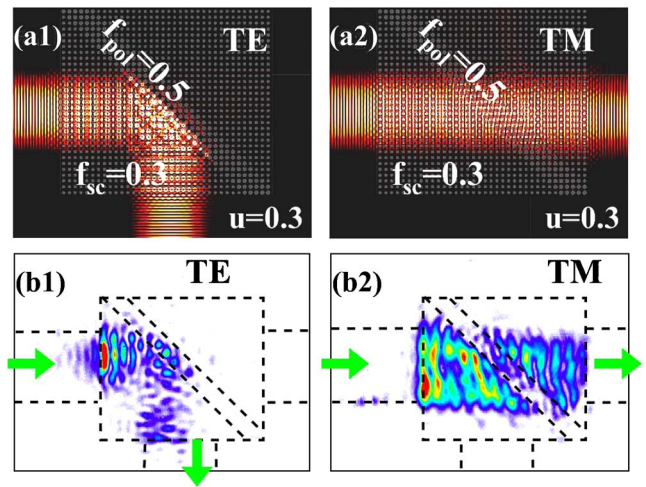


Fig. 2. (Color online) 2D FDTD modeling of (a1) TE and (a2) TM field patterns for the optimized self-collimating polarization splitter structure, showing transmission for TM light and high reflection for TE light. (b1), (b2) Top view from a high-numerical-aperture microscope image of the polarization splitter with TE and TM input polarization states; (b1) TE-polarized beam is reflected; (b2) TM-polarized field propagates through the splitter.  $\lambda=1.55 \mu\text{m}$ .

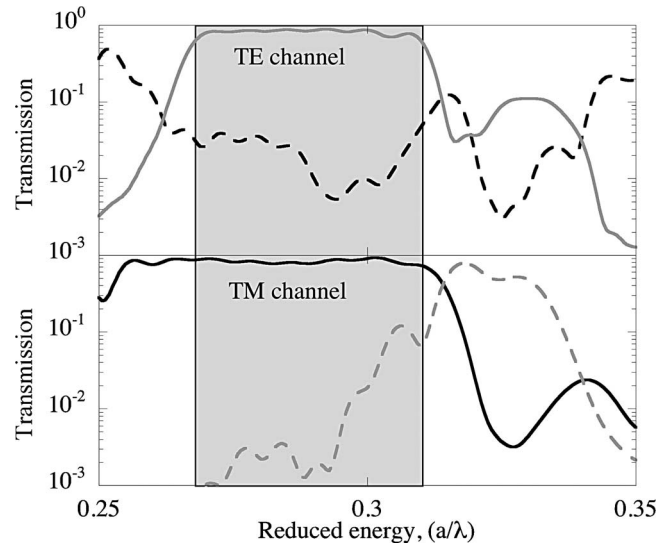


Fig. 3. Solid curve, 2D FDTD modeling of the (top) TE and (bottom) TM output spectrum of the optimized structure ( $f_{\text{st}}=30\%$  and  $f_{\text{pol}}=50\%$ ); dashed curve, cross-talk TE (TM) transmission in the TM (TE) channel.

specular location, which has to be taken into account in the final device design. The structures actually fabricated consist of a set of two splitters, with the first splitter performing the polarization separation itself while the second splitter reflects the TE beam, thus allowing the two polarizations to be measured through parallel ridge waveguides. The structures were fabricated in a single- and a dual-block version (see Fig. 4). Note that the TE measurements presented below are normalized to a single polarization splitter; i.e., the transmission spectra shown are the square roots of the measured spectra. The planar waveguide consists of an optimized GaInAsP/InP structure.<sup>12</sup> The lithography was performed on a

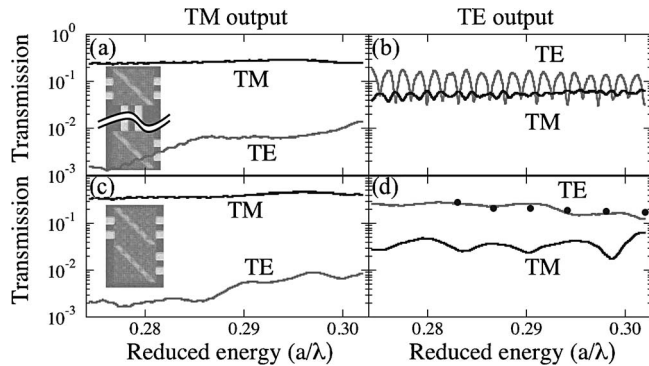


Fig. 4. Output spectrum of the polarization splitter (lattice constant=450 nm) in single (top) and dual (bottom) versions, TM (TE) channel left (right). TM, black; TE, gray. TE output is normalized to one device. Insets, microscope images of the single-block and dual-block version with or without an intermediate ridge waveguide.

LEO 1530/Raith Elphy electron-beam system, and structures were etched onto a custom-designed chemically assisted ion-beam etching (CAIBE) system by using Ar:Cl<sub>2</sub> and flowable oxide (FOX-12, Dow Corning) as the hard mask.<sup>13</sup> While the PhC section was deeply etched, the access waveguides were defined in a second lithography step and were shallow etched to ensure single-mode operation.

Measurements were performed on a regular end-fire setup with a tunable laser (range 1.47–1.66  $\mu\text{m}$ ) light source coupled into the sample via lensed optical fibers. Polarization control and analysis are inserted into the input and collection fibers. The samples as fabricated had filling factors close to the nominal values, as determined optically from calibration test structures. The transmission spectra for both output channels are shown in Fig. 4. The best results were obtained over a frequency bandwidth in excess of 5% and show an output transmission of 35% (25%–30%) for the TM (TE) channel with 0.2%–0.8% (3%–4%) TE (TM) cross talk in the TM (TE) output, respectively. The frequency range is likely to be larger, as the low-energy cutoff could not be measured owing to the limited wavelength range of the tunable laser for the given lattice constant of the sample. The free spectral range of the Fabry–Perot fringes in the dual-block version [Fig. 4(b)] agrees with the optical length corresponding to back-reflections at the tile interface or at the polarizing slab. The fringe contrast allows us to evaluate the reflection coefficient at 37% for TE and 10% for TM. The values obtained for the TE output were confirmed by an independent *in situ* measurement performed by N. Le Thomas and R. Houdré based on an analysis of the emission pattern of the light diffracted from the surface [black dots in Fig. 4(d)]. Figures 2(b1) and 2(b2) show the top view, high-numerical-aperture microscope image of the

polarization splitter with TE and TM input polarization states. The TM polarized self-collimated beam propagates through the splitter as expected, whereas the TE polarized beam is reflected.

Two mechanisms reduce the transmission of the polarization splitter: (1) out-of-plane light scattering, which can be either intrinsic, because the sample always operates above the light cone, or extrinsic, due to sample imperfections (hole shape or disorder); and (2) backreflection of the light at the interfaces (the ridge waveguide with the PhC tile or the polarizing slab). Improving the processing could reduce light scattering; however, this can be a demanding task, given that the present processing is already of high quality. Backreflected light could be reduced by improved design of the interfaces, including antireflective coatings with, for example, rows of increasing hole sizes. Considering that backreflection was estimated at 37% (TE) and 10% (TM), this gives a potential for improvement of transmission in the range of 45%–55% for the TM channel and 60%–90% for the TE channel, which are acceptable values for a marketable device.

The authors acknowledge support from the European projects Epixnet IST-004525, Funfox IST-004582, the COST P11 action and the Swiss “Quantum Photonics” National Center for Competence in Research. R. Houdré’s e-mail address is romuald.houdre@epfl.ch.

## References

1. T. Liu, A. R. Zakharian, M. Fallahi, J. V. Moloney, and M. Mansuripur, *IEEE Photon. Technol. Lett.* **17**, 1435 (2005).
2. Y. Kalra and R. K. Sinha, *Opt. Quantum Electron.* **37**, 889 (2005).
3. L. J. Wu, M. Mazilu, J. F. Gallet, and T. F. Krauss, *Appl. Phys. Lett.* **86**, 211106 (2005).
4. X. Y. Ao and S. L. He, *Opt. Lett.* **30**, 2152 (2005).
5. Z. H. Lu, Y. F. Tang, Y. F. Shen, X. H. Liu, and J. Zi, *Phys. Lett. A* **346**, 243 (2005).
6. V. Mocella, P. Dardano, L. Moretti, and I. Rendina, *Opt. Express* **13**, 7699 (2005).
7. S. Y. Kim, G. P. Nordin, J. B. Cai, and J. H. Jiang, *Opt. Lett.* **28**, 2384 (2003).
8. D. M. Pustai, S. Y. Shi, C. H. Chen, A. Sharkawy, and D. W. Prather, *Opt. Express* **12**, 1823 (2004).
9. H. Kosaka, T. Kawashima, A. Tomita, M. Notomi, T. Tamamura, T. Sato, and S. Kawakami, *Appl. Phys. Lett.* **74**, 1212 (1999).
10. P. T. Rakich, M. S. Dahlem, S. Tandon, M. Ibanescu, M. Soljacic, G. S. Petrich, J. D. Joannopoulos, L. A. Kolodziejski, and E. P. Ippen, *Nat. Mater.* **5**, 93 (2006).
11. B. Lombardet, L. A. Dunbar, R. Ferrini, R. Houdré, and F. Robin, *J. Appl. Phys.* **99**, 096108 (2006).
12. R. Ferrini, A. Berrier, L. A. Dunbar, R. Houdré, M. Mulot, S. Anand, S. de Rossi, and A. Talneau, *Appl. Phys. Lett.* **85**, 3998 (2004).
13. M. V. Kotlyar, L. O’Faolain, R. Wilson, and T. F. Krauss, *J. Vac. Sci. Technol. B* **22**, 1788 (2004).